# MIXED ORBITAL GROUND STATES OF $Fe^{2+}$ IN PRUSSIAN BLUES

A. I. Rykov,[1] J.Wang[1], T. Zhang[1], and K.Nomura[2]
[1]*Dalian Institute of Chemical Physics and Mössbauer Effect Data Center, Dalian 116023, China,* [2]*School of Engineering, The University of Tokyo, Hongo 7-3-1, 113-8656, Japan,*
(Dated: March 13, 2013)

We report on the mixed-orbital ground state compounds analogous to the mixed-valence ones. Orbital doublet and singlet ground states of the $Fe^{2+}$ ion displayed in Mössbauer spectra of the Prussian blue analogues $A_yFe_{3-y}[Co(CN)_6]_2 \cdot xH_2O$ ($y \leqslant 1$) are interconverting to each other as temperature changes for A = K, Na. Relative weight of orbital singlet ground states increases with lowering temperature. In the alcali-free cobalticyanides, the Mössbauer spectra are dominated by quadrupole-splt doublets of the same origin with a large splitting, characteristic of the $Fe^{2+}$ species coordinated by two (at least) oxygen atoms of water molecules in *cis*-configuration. Single-type octahedral $Fe^{2+}$ coordination is isolated in A-filled cobalticyanides for A=Rb, Cs to be characterized by the narrower quadrupole spectrum associated with the orbital doublet ground states. Ionic exchange of K for Cs in $KFe[Co(CN)_6] \cdot H_2O$ results in predominance of the orbital singlet, i.e., in enhanced anisotropy of the $Fe^{2+}$ valence electrons. We found hence that the $Fe^{2+}$charge distribution can be modified together with crystal size at the step of synthesis owing to distortion isomerism.

PACS numbers: 71.70.-d Level splitting and interactions; 76.80.+y Mössbauer effect;



## I. INTRODUCTION

Materials enclosing the transition metal elements are characterized by a wide diversity of ground states whether this be the quantum states of collective electron systems or local states. In latter case, the transitions between disparate ground states of 3d ions can be driven by changes in temperature, chemical doping, or by external stimuli. Phase transitions are thus induced that involve the spin, charge, lattice and orbital degrees of freedom. Charge transfer, spin crossover and linkage isomerism are the three types of transitions requiring a complex elucidation of the roles of corresponding degrees of freedom to be distinguished from each other[1–3]. The long-range structural aspects display their role via succession of transition steps as they evidence the interconversions between various local states mediated by elastic interactions[4,5]. Charge transfer from one site to another could be a prerequisite of the concomitant spin-state transition[6,7]. Orbital degree of freedom is responsible for a long-range-distortion symmetry lowering, provided that orbital ordering is coupled with the mixed-valence charge ordering transition[8]. Orbital ground state reversal[9,10] is an example of yet another type of transitions strongly coupled to the lattice and, possibly, to some other degrees of freedom. Simultaneous presence of the orbital singlet and orbital doublet ground states, familiar in case of $Fe^{2+}$ ion[11], could be an indication of proximity of such a transition.

Prussian blue (PB) analogues constitute a family of simple cubic compounds which excited a great interest recently owing to the family members exemplifying the spin crossover, charge transfer and linkage isomerism[1–3]. Here, in the same family, $A_yFe_{3-y}[Co(CN)_6]_2 \cdot nH_2O$ ($y \leqslant 1$, A = K, Na, Rb, Cs), we report on mixing and intercoverting the orbital ground states of $Fe^{2+}$.

Metal-organic framework of the PB analogues is formed by the 3d metal cations and the cyanometallate complex anions (of the $[Co(CN)_6]^{3-}$-type) arranged into a NaCl-like 3D checkerboard. In major group of these compounds, the valence and spin differ between the states of metal ions occupying the cationic node and the anion core. The framework complex anions are typically having higher valences than the cations, in this case, the framework is bearing a net negative charge, which is balanced either by insertion of alcali (A) cations into the framework interstitials or by spontaneous generation of the large-size vacancies on the anionic nodes. Crystallization and zeolitic water molecules (C-water and Z-water) fill the cavities at the vacant sites of complex anions and A-cations, respectively.

The local electronic configurations are probed by the quadrupole interactions of a $^{57}Fe$ Mössbauer nuclei sensing the electric field gradient from valent electrons and lattice charges surrounding the $Fe^{2+}$ ion. Mössbauer spectra of ferrous hexacyanocobaltates were reported previously only for the alcali-free phases ($y = 0$)[12,13]. The spectra can be fitted by two or more quadrupole doublets implying the existence of a number of different states of the high-spin $Fe^{2+}$ ions. Paired doublets, both originating from the cationic sites outside the low-spin complex $[M(CN)_6]$ were also observed in Mössbauer spectra of some other ferrous hexacyanometallates, e.g., for M=Cr ($y = 0$)[14]. The early Mössbauer study[12] has proposed that the water molecules in *cis-* and *trans-* configurations could contribute to the appearance of multiple sites for $Fe^{2+}$. In case of M=Cr, the spin-state transition of $Fe^{2+}$was observed only for $y \neq 0$ (A=Cs)[15]. It was conjectured[15] that filling the structure with A ions induces a stronger ligand field on the $Fe^{2+}$ ion that causes the spin transition. In this study of the local electronic configurations in $AFe[Co(CN)_6] \cdot H_2O$ ( A = K, Na, Rb, Cs) and related alcali-free form we show that the ligand field stabilizes the singular ground state (orbital doublet)

only for A=Cs and Rb. In the cases of A=Na, K, and $y = 0$ we report on the coexisting orbital singlet and orbital doublet ground states for $Fe^{2+}$ and on the interconversions between them induced by changes of temperature.

## II. EXPERIMENTAL

$RbFe[Co(CN)_6]\cdot H_2O$ and $CsFe[Co(CN)_6]\cdot H_2O$ were prepared mixing the 0.025 M aqueous solution of $K_3Co(CN)_6$with 0.025 M solutions of $FeCl_2\cdot 4H_2O$ in excess of RbCl or CsCl. Similarly synthesized samples in excess of KI and NaCl gave the compounds $K_{0.8}Fe_{1.1}[Co(CN)_6]\cdot H_2O$ and $Na_{0.7}Fe_{1.15}[Co(CN)_6]\cdot H_2O$, respectively. Analytic methods of inductively-coupled plasma and x-ray-fluorescent analysis gave the results consistent with the site occupancies obtained from Rietveld analysis. The same compounds with different crystal size were synthesized for A=Rb and Cs via the ionic exchange using $K_{0.8}Fe_{1.1}[Co(CN)_6]\cdot H_2O$ as a sorbent (Table I). Transformation of this sorbent into $CsFe[Co(CN)_6]$ was detected by Rietveld analysis and confirmed by analytic techniques.

**Table I.** Lattice parameters in the precipitated and ion-exchanged hexacyanocobaltates at room temperature.

| Compound | Parameter*, nm |
|---|---|
| $Na_{0.7}Fe_{1.15}[Co(CN)_6]\cdot H_2O$ | 1.03278(8) |
| $K_{0.8}Fe_{1.1}[Co(CN)_6]\cdot H_2O$ | 1.03115(3) |
| $KFe[Co(CN)_6]\cdot H_2O$ | 1.03107(3) |
| $RbFe[Co(CN)_6]\cdot H_2O$ | 1.03455(7) |
| $CsFe[Co(CN)_6]\cdot H_2O$ | 1.03682(8) |
| $Fe[Co(CN)_6]_{0.67}\cdot 5H_2O$ | 1.02778(8) |
| Cs-exchanged (b) at $20^oC$ | 1.03628(8) |

*Refined according to Fig.1 (c) and (d) structure models using the $Fm\bar{3}m$ space group.

X-ray Diffraction (XRD) patterns were measured on a PW3040/60 X'pert PRO (PANalytical) diffractometer using Cu Ka source. The atomic ratio Fe/Co and K/Co were determined by inductively coupled plasma atomic emission spectrometer (ICP-AES) on an IRIS Interpid II XSP Instrument (Thermo Electron Corporation). The x-ray fluorescent analysis was carried out using the XRF Axios X (PANalytical) spectrometer. The water content in the samples was estimated by thermogravimetric analysis carried out using a Setaram Setsys 16/18 analyser measuring the weight loss in an air flow of 25 ml/min with a heating rate of 10 K/min. Magnetization of the paramagnetic compounds was measured with a SQUID magnetometer in the range between 2 K to 350K.

Mössbauer spectra were measured with a Topologic 500 A spectrometer at the temperatures between 78 K and room temperature. The measurements at heating the sample above room temperature were performed in a Wissel GMBH furnace. Isomer shifts (IS) are reported relative to $\alpha$-Fe at room temperature.

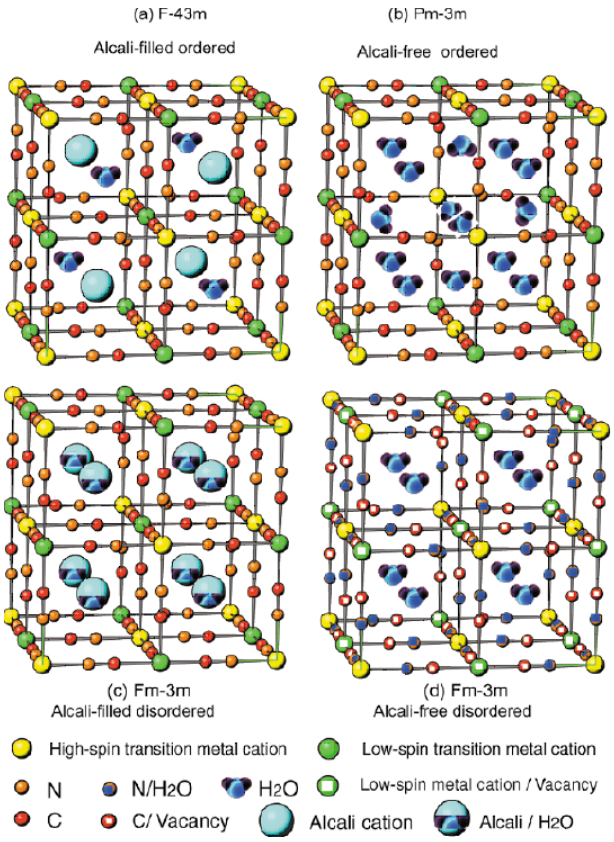


FIG. 1: Crystal structures and symmetry groups of the four modifications of Prussian blue analogues: alcali-filled ordered $F\bar{4}3m$ (a), alcali-free ordered $Pm\bar{3}m$ (b), alcali filled disordered $Fm\bar{3}m$ (c) and alcali-free disordered $Fm\bar{3}m$ (d).

## III. RESULTS AND DISCUSSION

### A. Structural considerations

The A-filled and A-free Prussian Blues are two types of the cubic frameworks, described by structure models of Keggin and Miles[16] and Ludi[17], respectively. Both of them exhibit the variable degrees of randomness in the distribution of the A ions over the framework interstitials and in the distribution of the water-filled anionic vacancies. In both cases, the *random* structures are described by the symmetry group $Fm\bar{3}m$. When the A-cations and Z-waters occupy the interstitials in an *ordered* fashion the symmetry turns into $F\bar{4}3m$. The $F\bar{4}3m$ symmetry appears, for example, in $CsFe[Cr(CN)6]\cdot H_2O$[15]. It means in the ideal case that the system of framework interstitials splits into two sublattices (1:1), as shown in Fig 1(a). In reality, each of these (1:1) sublattices is not represented by solely A-ions and Z-waters, but occupied just unequally with these two species.

In the A-free structure, another sublattice may split into two subsystems that is the anionic sublattice. When one proceeds from the disordered to ordered placement

of anionic vacancies the symmetry turns from $Fm\bar{3}m$ to $Pm\bar{3}m$ giving birth to two dissimilar sublattices[18]. In the $Pm\bar{3}m$ structure, two born sites are abundant with the ratio of 3:1. Four relevant lattice cells are shown in Fig.1 for the pairs of A-free and A-filled structures.

Rietveld refinements were carried out using the above mentioned four structural models and three symmetry groups known from the literature[16–19]. These treatments have shown that the most symmetric $Fm\bar{3}m$ model is sufficient to fit all the observed reflections. When fitted with lower symmetries the XRD least-square analysis has resulted in stagnant goodness of fit, unimproved, despite larger number of fitting parameters. The intensity ratio $I_{200}/I_{220}$ changes dramatically when K, Rb or Cs ions enter into the structure, as reported previously[20]. The change becomes very large as the number of electrons in an alcali ion increases, allowing for Cs a rough estimation of its content even prior to Rietveld analysis.

The refined lattice parameters at ambient temperature are listed in Table I. In all compounds, the lattice parameter is close to that of the low-spin phase of $CsFe[Cr(CN)_6]\cdot H_2O$[15], however, it is found from magnetic measurements that the addressed in Table I compounds enclose the $Fe^{2+}$ ions in the high-spin state that is unchanged down to 2 K.

### B. Doublet and singlet orbital ground states of $Fe^{2+}$ in PB analogues

#### 1. *Splitting the d-orbital energy level in anisotropic environment*

In the fully A-filled PB analogues, the $Fe^{2+}$ ions are coordinated with six nitrogens, however, at partial filling at least one C-water molecule enters the first coordination sphere of $Fe^{2+}$. From the combined scheme of compensating the charge misbalance between $Fe^{2+}$cations and $Co(CN)_6]^{3-}$ anions this is evidently the case of our samples (Table I). Electronic configuration of a high-spin $d^6$ ion implies only one electron extraneous with respect to isotropic half-closed d-shell composed of five spins-up electrons. In an octahedral environment, the group of three $t_{2g}$ orbitals is available for this sixth electron. We show in Fig. 2 the orientations of these orbitals relative to the water molecule.

The values of chemical shifts for both doublets in Fig. 3 are in the range 1.1 mm/s to 1.15 mm/s allowing us to identify indeed both doublets with the high-spin $Fe^{2+}$. In case of high-spin $Fe^{2+}$, the valence contribution of the electric field gradient (EFG) is predominant and exceeds the lattice EFG term by an order of magnitude[21]. The $t_{2g}$ group is thus the source of valence term of EFG that is the main contribution of the observed quadrupole splitting.

One of the orbitals of the $t_{2g}$ group in Fig.2 (a,b,c) is perpendicular to the direction pointing towards the water molecule. Corresponding energy level would not be affected by the ligand replacement. The lobes of two other orbitals ($d_{xz}$ and $d_{yz}$ in Fig.2) are at 45° with respect to oxygen direction. Owing to reduced repulsion between oxygen and $d_{xz}$ or $d_{yz}$ electrons corresponding levels would have lower energy. In the ground state of $Fe^{2+}$ ion, these $d_{xz}$ and $d_{yz}$ share the sixth d-electron (spin-down electron), while five spin-up d-electrons span isotropically. The third ($d_{xy}$) orbital would split off its energy level upwards from the ground state, formed by two degenerate $d_{xz}$ and $d_{yz}$ orbitals as shown in Fig. 2(d).

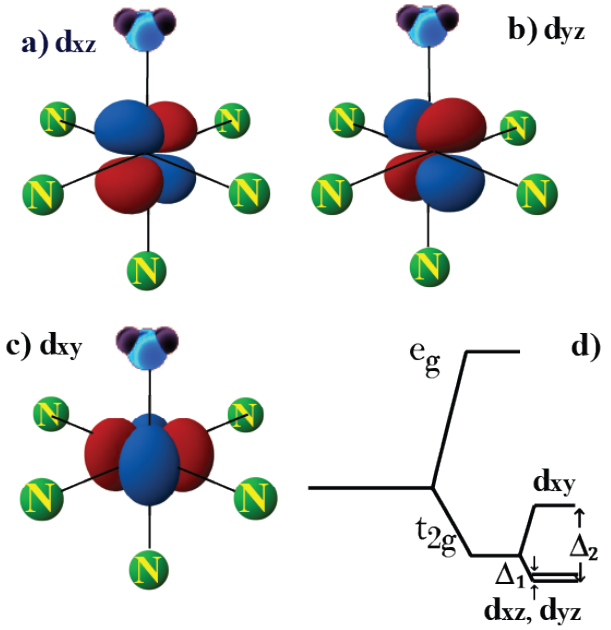


FIG. 2: Formation of the orbital doublet ground state of $Fe^{2+}$ in the "5+1" environment. In a Prussian Blue analogue, the valence spin-down electron clouds are depicted for the $Fe^{2+}$ species coordinated by 5 nitrogens and one water molecule. It is shown that two orbitals of the $t_{2g}$ group ($d_{xz}$,$d_{yz}$) retain the equivalent energy (a,b), whereas the third one (c) splits off upwards. A single spin-down electron occupies the double-degenerate level forming the doublet orbital ground state.

#### 2. *Temperature dependence of quadrupole splitting in A-filled cobalticyanides (A=Na,K):*

We observe in Fig. 3 two doublets, both of them having the temperature-dependent quadrupole splitting. In addition, the ratio of doublet areas is also strongly temperature-dependent. The external doublet is dominating at low temperatures. As the temperature is raised an inverted doublet area ratio is observed. Mössbauer spectra show that the triple degeneracy of $t_{2g}$ is lifted over either in favor of the orbital singlet or in favor of orbital doublet ground states. The charge distribution is less anisotropic when the spin-down electron is shared between two orbitals as shown in Fig.2. We as-

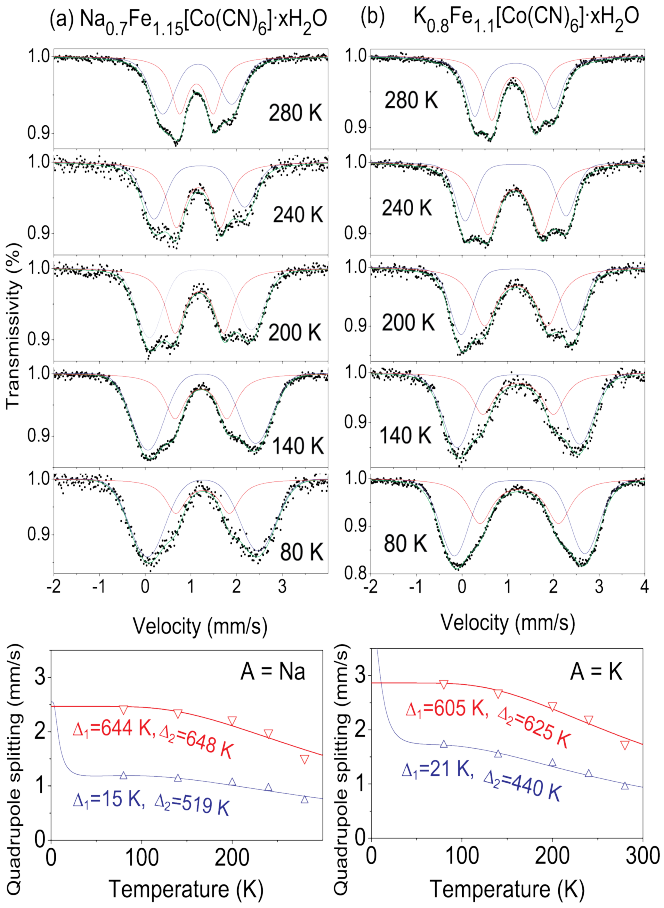


FIG. 3: Mössbauer spectra of the A-filled ferrous hexacyanocobaltates for A=Na and K in temperature range between 80 K and 280 K. In the bottom panels, the experimental temperature dependences of the quadrupole splittings determined from least-squares fitting the Mössbauer spectra are shown by triangle symbols. The solid lines represents $\Delta E_{\rm Q}(T)$ fitted using Eq.(1) with the parameters $\Delta_1$ and $\Delta_2$ indicated.

cribe such a charge state to the internal doublet of Fig.3. Larger charge anisotropy originates from localizing the sixth electron of $Fe^{2+}$ on a single *d*-orbital (external QS doublet). From the QS ratio the valence EFG term is expected to be twice larger for the orbital singlet than for the orbital doublet. The literature overview confirms indeed that in $Fe^{2+}$ the orbital singlet produces twice larger quadrupole splitting than the orbital doublet ground state[9,11,21–24].

In the bottom of Fig. 3, we fitted the values of $\Delta E_{\rm Q}$ derived from Mössbauer spectra with the theoretical expression[24]:

$$\Delta E_{\rm Q}(T) = \Delta E_{\rm Q}^0 \frac{1 + e^{\frac{-2\Delta_1}{k_{\rm B}T}} + e^{\frac{-2\Delta_2}{k_{\rm B}T}} - e^{\frac{-\Delta_1}{k_{\rm B}T}} - e^{\frac{-\Delta_2}{k_{\rm B}T}} - e^{\frac{-(\Delta_1+\Delta_2)}{k_{\rm B}T}}}{1 + e^{\frac{-\Delta_1}{k_{\rm B}T}} + e^{\frac{-\Delta_2}{k_{\rm B}T}}} \quad (1)$$

Here $\Delta E_{\rm Q}^0$ is the quadrupole splitting at zero temperature, which can be as high as 3.7 mm/s for $Fe^{2+}$[25]. The fitted values of the energy gaps $\Delta_1$, $\Delta_2$ are also shown in Fig.3.

The ratio of the fitted values $\Delta_1 : \Delta_2$ is small ($\sim 0$) and large ($\sim 1$) for the internal and external QS subspectra, respectively. This is consistent with the subspectra assignment to the orbital doublet and orbital singlet ground states identified according to their QS values. Very small splitting $\Delta_1$ ( $\ll \Delta_2$ ), similar to fitting error, is allowed between the $d_{xy}$ and $d_{xz}$ levels. Even if this degeneracy is locally lifted by some remote disorder, such small splitting $\Delta_1$ remains unobservable until very low temperatures. On the other hand, the effect of larger $\Delta_2$ is the robust steepness of the QS vs. $T$ dependence troughout a broad temperature range. Similar splitting of 340 $cm^{-1}$ ($\approx$ 490 K) was estimated in $Fe_3[Co(CN)_6]_2 \cdot 5H_2O$ by Rasmussen and Meyers[12].

### 3. *Classification scheme of the $Fe^{2+}$ sites by the symmetry of environment*

Our Rietveld refinements in both A-filled and A-free series of cobalticyanides have revealed that their structures are best described by the symmetry $Fm\bar{3}m$, allowing for the $Fe^{2+}$ ion a number of different coordination environments. The $Fe^{2+}$ sites can be classified by the number and configuration of N-ligands replaced with $H_2O$. In these $Fe^{2+}$ sites, the lowest in energy state depends on the $H_2O$ inclusion in first coordination sphere, however, when $H_2O$ is not included, the ground state is determined by the local distortion. Owing to so-called distortion isomerism[9] the ground state becomes not uniquely defined. Shown in Fig.4 are the cases of distortion isomerism (a), orbital singlet (b), and orbital doublet (c).

The distortion isomerism is the phenomenon closely related to the inability for the sixth (spin-down) electron to be distributed isotropically over the triply degenerate $t_{2g}$ orbital. Such an overmuch triple degeneracy is universally lifted over by a local distortion of one or another type. In a $FeN_6$ octahedron, the compression along tetragonal axis would stabilize the orbital singlet lowest (a-1), while elongation along tetragonal axis stabilizes the orbital doublet as a ground state (a-2). Opposite effects are expected for the compression and elongation along the trigonal axis of the octahedron[23]. Self-coupling

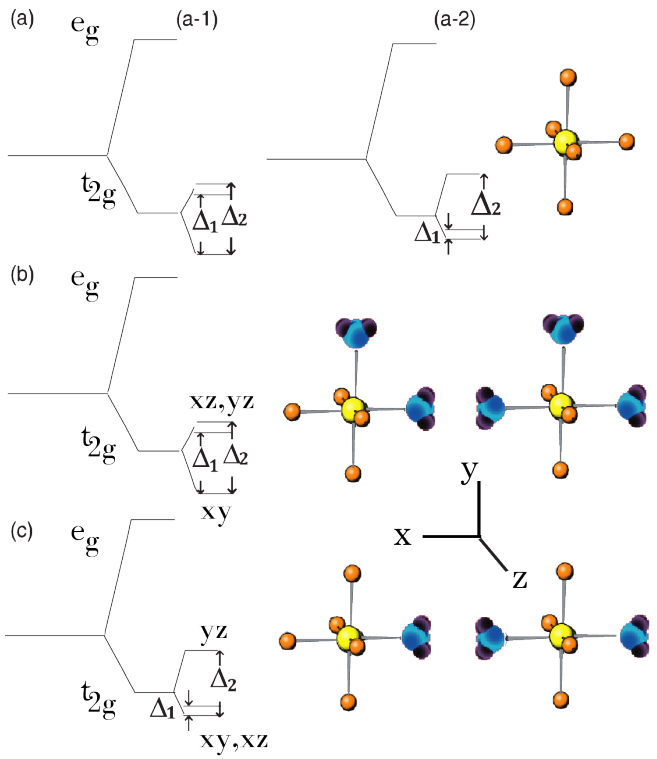


FIG. 4: Energy level diagrams and corresponding coordinations for the orbital singlet (a-1) and (b) and orbital doublet (a-2) and (c) ground states of the $Fe^{2+}$ ion in ferrous hexacyanocobaltate. In a-1 (a-2) the diagram of level splitting for the distorted $FeN_6$ ocahedron is shown for the elongation (compression) along tetragonal (trigonal) axis.

between electron localization and local distortion eliminates the case of zero EFG valence term that is never observed.

This physical picture is a key to understanding the temperature variation of the abundance of two Mössbauer doublets in Fig. 3. Assuming that the 6N-coordinated $Fe^{2+}$ sites are contributing to both doublets, we observe that the relative abundance of the orbital doublet and orbital singlet states is varying with temperature owing to varied lattice distortion. Matsuda et al[26] have reported that the PB lattice possess an intrinsic instability with respect to rotations of the rigid units of the $[Co(CN)_6]^{3-}$-type. The rotational displacements generate spontaneously to stabilize the excited charge-transferred states, which arises owing to strong lattice-electron coupling. The same rotational displacements cause also the negative thermal expansion[26]. Recently, the thermal expansion in $Fe_3[Co(CN)_6]_2 \cdot nH_2O$ was reported to be indeed negative, at least above 200 K[27].

We observe thus that the orbital ground state reversal accompanies the distortion isomerism. One or another of coexisting distortion isomers prevails in a particular temperature range. Largest charge anisotropy occurs at lower temperatures owing to localizing the sixth electron of $Fe^{2+}$ on a single $d$-orbital. The charge distribution is less anisotropic at higher temperatures when the spin-down electron is shared between two orbitals. The temperature variation of the abundance of two Mössbauer doublets is very smooth. Similar temperature-varied local distortion concurrence that engenders the distortion isomerism was observed previously[9]. The glasslike transition driven by supercooling $\Delta T$ was characterized[23] by an equilibration time which decreases smoothly with temperature. The distortion switch-over is local and distributed over a broad temperature range.

With decreasing the content of A-ions the anionic vacancies (water-filled pores) are generated for charge compensation. When the pore concentration is small only populated are the $Fe^{2+}$ sites which contain one $H_2O$ ligand as shown in Figs. 2 and 4(c). Two pores in a vicinity of a $Fe^{2+}$ species occur either in *trans-* or in *cis-* configurations. Consider in Fig. 4(c), for example, the ground state of the *trans-* $Fe^{2+}$. If we denote by $x$ the direction from the central $Fe^{2+}$ ion towards two *trans-* $H_2O$ ligands then the lobes of both $xy$ and $xz$ orbitals would be pointing to directions having an angle of $45^o$ with the $x$ axis. The lobes of the third $t_{2g}$ orbital ($yz$) would be pointing to the direction orthogonal to the $x$-axis. Therefore the ground state of the $Fe^{2+}$ ion in such $FeN_4(H_2O)_2$ octahedron would be the orbital doublet. This is the same ground state as shown in Fig. 2 for the $Fe^{2+}$ ion in the $FeN_5H_2O$ octahedron with a single water in first coordination sphere. Orbital singlet in Fig. 4(b) is the ground state corresponding to the *cis-*configuration of $FeN_4(H_2O)_2$ and to the octahedron with three in-plane waters.

The $H_2O$ placement into the first coordination sphere of $Fe^{2+}$ suppresses the distortion isomerism and stabilizes a singular ground state of $Fe^{2+}$. In our samples $Na_{0.7}Fe_{1.15}[Co(CN)_6]\cdot H_2O$ and $K_{0.8}Fe_{1.1}[Co(CN)_6]\cdot H_2O$ the density of anionic vacancies is rather small and the population of the $Fe^{2+}$ ions surrounded by two vacancies is also small. In these samples the inner doublet comes from the $Fe^{2+}$ orbital doublet ground state associated with the $FeN_5H_2O$ octahedron and with one of distortion isomers of $FeN_6$. The outer doublet comes mainly from another distortion isomer of $FeN_6$ having the orbital singlet ground state.

### *4. A-filled cobalticyanides (A=Rb,Cs)*

Another manifestation of distortion isomerism is the difference between the Mössbauer spectra of the A-filled cobalticyanides obtained for Rb and Cs by two different procedures. Using the standard technique, the A-filled cobalticyanides were obtained by precipitation method. These compounds have demonstrated the single-component Mössbauer spectra (a) and (b) in Fig.5, identified with orbital doublet ground state. On the other hand, when the method of ionic exchange was applied to replace K by Cs in $KFe[Co(CN)_6]\cdot H_2O$, the second QS

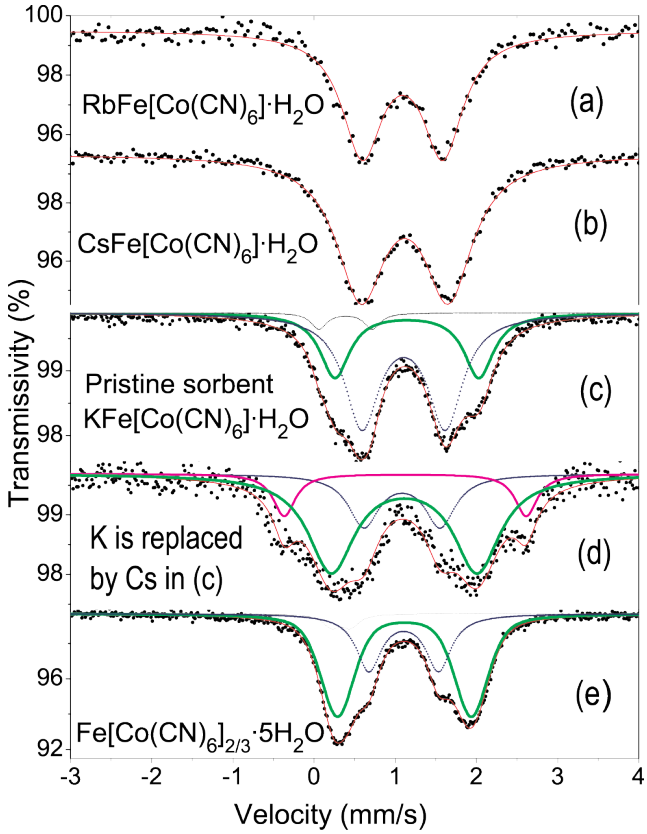


FIG. 5: Mössbauer spectra of the A-filled ferrous hexacyanocobaltates obtained in three different procedures: precipitation (a-c,e), and ionic-exchange (d). The spectra fitting parameters are listed in Table II.

subspectrum, identified with the orbital singlet, did not disappear. On the contrary, we observed the strong enhancement of the outer doublet with $\Delta E_Q$=1.8 mm/s, from 32% to 64%. In addition, there appears a component (13%) with extremely large $\Delta E_Q$ of 3 mm/s. It is assigned to another orbital singlet state with larger energy level splitting parameters $\Delta_1$, $\Delta_2$. The difference between two external doublets of the sample (d) is a manifestation another type of distortion isomerism unrelated to switching between different orbital ground states[28].

Rietveld refinements resulted in similar compositions for two different syntheses. The intensity of x-ray diffraction has very similar patterns, except linewidth difference. Larger-size crystallites of $CsFe[Co(CN)_6]\cdot H_2O$ are obtained via ionic exchange. In this method, the crystal size of is $CsFe[Co(CN)_6]\cdot H_2O$ is determined by the size of the $KFe[Co(CN)_6]\cdot H_2O$ precursor crystals. The target compound $CsFe[Co(CN)_6]\cdot H_2O$ with such large crystals could not be obtained by the standard method of precipitation from a solute. Despite of similarity of the x-ray patterns, the QS of the ion-exchanged and precipitated samples of $CsFe[Co(CN)_6]\cdot H_2O$ indicates that the valent spin-down electron has a very different distributions over the orbitals of $t_{2g}$ group (Table II).

**Table II.** Parameters of Mössbauer spectra (Fig. 5) in as-synthesized (a-c) and (e) and Cs-sorbed(d) hexacyanocobaltates: isomer shift (IS) $\delta$, quadrupole splitting (QS) $\Delta E_Q$, linewidths $\Gamma$(mm/s), and spectral abundance (%).

| Compound | $\delta$(mm/s) | $\Delta E_Q$ (mm/s) | $\Gamma$(mm/s) | % |
|---|---|---|---|---|
| (a):$RbFe[Co(CN)_6]\cdot H_2O$ | 1.091(5) | 0.992(8) | 0.60(1) | 100 |
| (b):$CsFe[Co(CN)_6]\cdot H_2O$ | 1.116(3) | 1.077(4) | 0.71(1) | 100 |
| (c):$KFe[Co(CN)_6]\cdot H_2O$ | 1.144(3) | 1.77(1) | 0.44(2) | 32 |
| | 1.104(2) | 1.03(1) | 0.52(2) | 64 |
| | 0.39(1) | 0.66(2) | 0.23(3) | 5 |
| (d): ion-exchanged K for Cs in (c) | 1.111(5) | 1.80(3) | 0.69(4) | 64 |
| | 1.084(9) | 0.94(3) | 0.45(4) | 23 |
| | 1.123(8) | 2.98(2) | 0.33(4) | 13 |
| (e):$Fe[Co(CN)_6]_{2/3}\cdot 5H_2O$ | 1.114(2) | 1.65(1) | 0.45(1) | 64 |
| | 1.104(2) | 0.86(1) | 0.38(1) | 31 |
| | 0.33(1) | 0.23(2) | 0.26(3) | 5 |

We observe in the standard (not ion-exchanged) compounds that only one type of the octahedron distortion is preferred when the large-size A-ions occupy the interstitials, and this type of distortion stabilizes the orbital doublet lowest. On the other hand, in the case of A=K or A=Na the appearance of the outer doublet comes into play. In this series of PB analogues, several related aspects of structure and properties turn out to be A-size-dependent. Whereas in the case Cs(Rb)-containing PB analogue compounds the Cs(Rb) ions are situated in the centers of the interstitial cubes, in the case of some K(Na)-containing compounds the K(Na) ions are reported to be eccentrically located[29]. The mobility of alkali metal ions in the channels of the hexacyanometalate structure decrease dramatically with increasing the alcali ionic radius[29]. The irreversible fixation of the less mobile ions ensures the Cs-selectivity for the cobalticyanide sorbents, allowing the ionic exchange to be used in practice for $^{137}$Cs removal from radioactive wastes[30,31].

### 5. *Alcali-free ferrous cobalticyanide*

The isomer shifts in Mössbauer spectrum the A-free $Fe[Co(CN)_6]_{2/3}$ (Fig.5e) indicates predominantly (95%) the high-spin $Fe^{2+}$. The ground states of the major part of the $Fe^{2+}$ species (64%) are the orbital singlet states. Third minor doublet is assigned to $Fe^{3+}$ according to its isomer shift and magnetic measurements. Refinements of the structure of $Fe_{1.5}[Co(CN)_6]\cdot H_2O$ were useful to confirm the assignments of three $Fe^{2+}$ Mössbauer subspectra to the defined structural sites. Let us consider first the structure models of archetype Prussian Blue investigated previously[18,32]. The concentration of pores in the A-free hexacyanocobaltate is very large, therefore, they cannot be considered as isolated ones. All kinds of

associations between the water-filled pores underlie the resulting abundance of the $Fe^{2+}$ species in various coordinations. Interactions between the pores at the stage of synthesis may result in various distributions of the pores. For the Prussian Blue $Fe_4[Fe(CN)_6]_3 \cdot 14H_2O$, depending on the growth conditions, Buser et al[18] could synthesize the single crystals with varied degree of disorder. Structures of several crystals were refined using the $Fm\bar{3}m$ model, others were best refined using the $Pm\bar{3}m$ model. *A priori*, only fully randomized distribution of the pores is consistent with the $Fm\bar{3}m$ model (Fig. 1d). Low symmetry ($Pm\bar{3}m$) becomes applicable when one finds unequal occupancies for the cell body center and edge centers (Fig. 1b). These sites are abundant with the ratio of 1:3. If $p$ is the occupancy of the body center, and $1 - p/3$ is the occupancy of the edge centers, the conditions $p = 0$ and $p = 3/4$ correspond to fully ordered and random PB structures, respectively[18]. In ferrous hexacyanocobaltate, owing to different valence ratio the same conditions correspond to $p = 0$ and $p = 2/3$. Intermediate partially-ordered structures can be characterized by the order parameter $\gamma = 1 - 3p/2$ .

In Fig. 6, we have calculated the abundance of various coordinations of $Fe^{2+}$ for several values of $\gamma$ between 0 and 1. The total abundance of the $Fe^{2+}$species in the orbital doublet ground state $A_D$ is made up mainly of the abundances of $FeN_5H_2O$ and *trans*-$FeN_4(H_2O)_2$. Relatively small number of water-free octahedra $FeN_6$ is assumed to be halved between two distortion isomers.

Abundance of the orbital singlet $A_S$ is composed *cis*-$FeN_4(H_2O)_2$, $FeN_3(H_2O)_3$ and remaining $FeN_6$(distortion isomer). Both in-plane and 3D ligand configurations in the 3:3 octahedron $FeN_3(H_2O)_3$ contribute to $A_S$. First, when 3 oxygens coordinating to iron are in one plane the $x$, $y$ and $z$ axes become all nonequivalent. In this case, the spin-down electron cloud loses the axial symmetry, and the $t_{2g}$ group splits into three singlets. Second, when three oxygens are in 3D configurations, all three axes $x$, $y$ and $z$ are equivalent; nevertheless, the cubic symmetry is lost. Since $H_2O$ is a weaker ligand than N this geometry can be viewed as an octahedron with three ligands expelled to longer distance than other three. Equivalent spatial distortion is the elongation along the trigonal axis. Such a distortion was shown to stabilize the orbital singlet lowest[9].

As $\gamma$ decreases, the integral value of $A_D$ shows in Fig. 6 the percentages of 63%, 52%, 44%, 39% and 38% for $\gamma = 1, \frac{3}{4}, \frac{1}{2}, \frac{1}{4}, 0$ , respectively. Main trend of reduction of $A_D$ is determined by the reduction of the *trans*-subpopulation of $FeN_4(H_2O)_2$. The orbital singlet ground state prevails in the disordered structure described by the $Fm\bar{3}m$ model. In this case ($\gamma = 0$), the expected area of the external doublet $A_S$ reaches the value of 62% similar to experimental result of 64% in Table II.

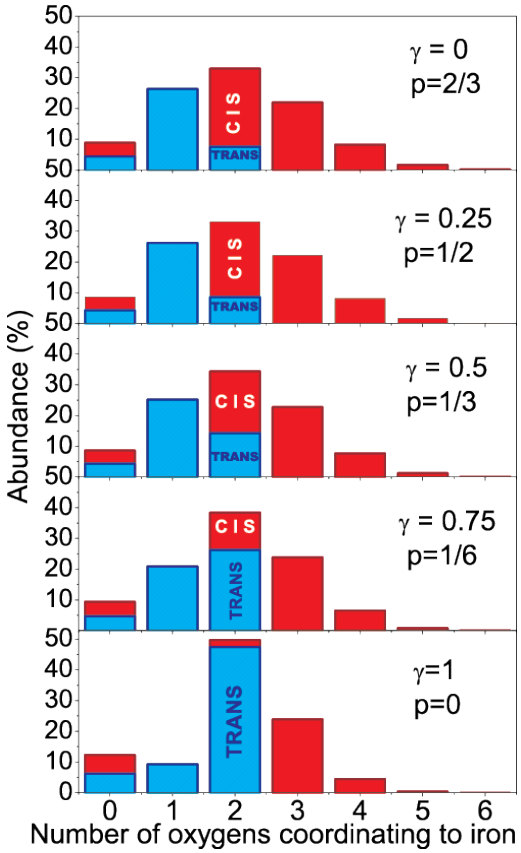


FIG. 6: Evolution of the distribution of abundances of the coordination polyhedra $FeN_{1-n}O_n$ ($n = 0, 1, 2, 3, 4, 5, 6$) as the structure randomizes starting from order parameter $\gamma = 1$ ($Pm\bar{3}m$ model, Fig1,b) to $\gamma = 0$ ($Fm\bar{3}m$ model, Fig.1 d). Here $p = 2(1-\gamma)/3$ is the occupancy of the center of the cubic cell in Fig.1 (b). Total abundances of orbital singlet and orbital doublet ground states are distinguished by color.

### C. Models of short-range order in PB analogues

The concentration of pores in archetypal Prussian Blue, ferric ferrocyanide $Fe[Fe(CN)_6]_{1-\delta} \cdot 3.5H_2O$, is $\delta = 1/4$, so that the ratio $1 - \delta : \delta$ is 3: 1. The ordered $Pm\bar{3}m$ structure proposed for Prussian Blue in Ref.[18] contains the high-spin cations only in coordinations $FeN_6$ (25%) and trans-$FeN_4(H_2O)_2$ (75%). In ferrous hexacyanocobaltate, the ratio $1 - \delta : \delta$ is 2: 1. Therefore, for a vacancy-ordered phase of such a stoichiometry one cannot expect the same set of coordinations as for the $Pm\bar{3}m$ structure of the Ref.[18].

In order to construct an ordered phase with the ratio $1 - \delta : \delta$ of 2: 1 we try to fill 3 sites with Fe, 2 sites with Co, 1 site with Co vacancies, and 0 sites with Fe vacancies. We find that among cubic structures of NaCl-type there is no superstructure with exact site ratio 3:2:1:0, however, a unique superstructure with the ratio of 30:20:12:2 exists. Using the body-centered $Im\bar{3}m$ model we can develop the proper arrangement of the va-

cancies with a variable order parameter. Table III shows the details of the fully ordered ($\gamma = 1$) Im$\bar{3}$m structure. The order parameter $\gamma = 1-8p/3$ is defined via the occupancy $p$ of the (12e) position that is the core of complex anion $[Co(CN)_6]^{3-}$.

**Table III.** Wyckoff positions, atom type, relative coordinates and occupancies of the Na and Cl nodes in the superstructure Im$\bar{3}$m model on the basis NaCl-type framework.

| Wyckoff | Atom | x | y | z | Occ. |
|---|---|---|---|---|---|
| 2a | Fe | 0 | 0 | 0 | 0 |
| 6b | Fe *Trans* | 0 | 1/2 | 1/2 | 1 |
| 8c | Co | 1/4 | 1/4 | 1/4 | 1 |
| 12d | Co | 1/4 | 0 | 1/2 | 1 |
| 12e | Co | 1/4 | 0 | 0 | 0 |
| 24h | Fe *Cis* | 0 | 1/4 | 1/4 | 1 |

Among total 14 vacancies per cubic cell of the Im$\bar{3}$m structure (Table III) we place 12 vacancies of the complex anion $Co(CN)_6$ and 2 cationic ($Fe^{2+}$) vacancies. We obtained the ordered structure of $Fe[Co(CN)_6]_{2/3}\cdot\frac{85}{16}H_2O$ which contains 2 very large cross-shaped pores (6+1-pores, or +-pores). Each cationic vacancy is surrounded by 6 anionic vacancies. The hydration degree $\frac{85}{16}$ is calculated assuming 14 water molecules per standard pore and an additional water molecule per $Fe^{2+}$ vacancy. Thus, the 6+1-pore is composed of 6 standard pores aggregated into 3D crosslike body. The edge of the Im$\bar{3}$m cell is twice longer than the edge of the Pm$\bar{3}$m cell and the cell volume is 8-fold.

The body-centered Im$\bar{3}$m model exhibits only two kinds of $Fe^{2+}$ sites with the abundance ratio of 3:1, similar to that of the Pm$\bar{3}$m model. In both models, the major site (75%) is coordinated with two waters. However, in the Pm$\bar{3}$m model the major site is coordinated by waters in *trans*-configuration, whereas in the Im$\bar{3}$m model the major site is coordinated by waters in *cis*-configuration. The minor site in Pm$\bar{3}$m model is coordinated by six nitrogens, and in Im$\bar{3}$m model by four nitrogens and two waters in *trans*-configuration.

It is important that we were able to construct the superstructure model, which strongly favors the *cis*-configuration in agreement with prevailing external doublet in Mössbauer spectra. Although the random Fm$\bar{3}$m model agrees as well with the experiment, the lack of any short-range order between pores appears to be a severe limitation of this model because the vacancies bearing a charge interact with each other repulsively. We must note also that the luck of any superstructure reflections in diffraction patters may not be an evidence of a missing short-range order, but only the evidence of lacking *long-range* order. The suggested Im$\bar{3}$m structure is a plausible model of the short-range order in the mixed-valence 2:3 PB analogues.

Although the superstructure reflections, predicted by either Pm$\bar{3}$m or Im$\bar{3}$m models, were not observed by x-ray diffraction, using the probabilities of local structure patterns observed by such a local technique as Mössbauer spectroscopy one can identify the proper model of short-range order. The Im$\bar{3}$m model predicts the strong predominance (3:1) of *cis*- over *trans*- population among the $Fe^{2+}$ environments. The model describes the situation when concentration of elementary vacancies is so high that they must be in small clusters. In contrast, the Pm$\bar{3}$m model describes the limit when all vacancies are still isolated, however, no more vacancies can be added without clustering. If they are actually added to proceed from $\delta = 1/4$ to $\delta = 1/3$ (as in the bottom panel of Fig.6), there will result the extra-holey Pm$\bar{3}$m model that fails to describe the Mössbauer spectral data. In our experiments, we observe the prevailing abundance of the *cis*-configurations related to the extended crosslike pores. The aggregation of small pores into extended pores underlies the large (up to 750 $m^2/g$) specific surface and unique gas sorption properties of these materials[33].

### D. Charge-transferred states in the PB analogues

The charge-transferred states which were discussed above to induce the distortion isomerism are seen in the third small (5%) doublet with IS of $Fe^{3+}$ in Fig.5 (c) and (e). A slight asymmetry appears also in Fig.3, although these spectra were fitted without introducing explicitly the $Fe^{3+}$ component. The pairs of $Fe^{2+}/Co^{3+}$ and $Fe^{3+}/Co^{2+}$ can be considered as valence tautomers, and we explain the asymmetry in these spectra by electron transfer from $Fe^{2+}$ to $Co^{3+}$. The formation and rupture of the chemical bonds implies no migration of atoms but only migration of electrons. The cobalt ions remain in low-spin state as the sixth electron of $Fe^{2+}$ transfers from $t_{2g}$ orbital of $Fe^{2+}$ to $e_g$ orbital of $Co^{2+}$. Other compound susceptible to valence tautomerism were known previously[19,34]. For example, the Prussian Blue analogue $RbMn[Fe(CN)_6]\cdot H_2O$, when synthesized in excess of Rb to fill enough framework interstitials with Rb, crystallizes in the structure shown in Fig. (1a). In this system, the tautomers $Fe^{2+}/Mn^{3+}$and $Fe^{3+}/Mn^{2+}$ are able to form different crystal phases which give way to each other as temperature changes.

In the ferrous cobalticyanides, no abrupt phase change was found to be caused by the charge-transferred states. On the other hand, we observed that the content of $Fe^{3+}$ can be changed depending on the excess of $FeCl_2$ and dilution degree in the course of precipitation of $Fe[Co(CN)_6]_{2/3}\cdot 5H_2O$. Rapidly synthesized compound contained up to 15-20% of $Fe^{3+}$, however, the content of $Fe^{3+}$ was reduced down to just 5% through reducing the reaction rate in dilute solutions. Most probably, the lack or misplacement of water molecules is needed to stabilize locally the charge-transferred states and make them observable in Mössbauer spectra. It appears in this case that the rapidly prepared samples are not saturated in C-water. The sites of $Fe^{2+}$ nearest to the nodes lacking the coordination water are subject of local tautomer transformation. In a slowly synthesized $Fe_{1.5}[Co(CN)_6]\cdot 5H_2O$ such crystallization defects are reduced.

Measuring the Mössbauer spectra above room temperature supports this concept. With raising temperature the area of the $Fe^{3+}$ subspectrum starts to increase irreversibly. Thermogravimetric analysis showed that the loss of sample weight occurs at heating practically starting from room temperature. The Mössbauer spectrum measured *in situ* in a furnace at 318 K shows the area of the $Fe^{3+}$ doublet increased up to 37%. The same sample measured *ex-situ* after prolonged (1 week) heat treatment at $60^oC$ showed the area of the $Fe^{3+}$ increased up to 57%. The equilibrium hydration degree at $60^oC$ is related with nearly half iron species transformed to $Fe^{3+}$. Longer exposure in air at at $60^oC$ induces no further increase of the spectral asymmetry and the area of spectral component with IS of 0.39 mm/s remains at the level of 57%.

The isomer shift of 0.39 mm/s is attributable, in principle, either to high-spin $Fe^{3+}$ or to low spin $Fe^{2+}$. The latter was observed below the spin-state transition in $CsFe[Cr(CN)_6]$[15]. Theoretical approaches to lattice-dynamic calculations[35],[36] show that the change in the electronic state is closely related to the structure expansion as the lattice parameter grows between the low-spin and high-spin forms from 1.03 nm to 1.07 nm. In $Fe_3[Co(CN)_6]_2 \cdot nH_2O$, the thermal lattice expansion is negative[27]. To verify that we do not deal with a *reverse* spin transition[37,38], we have compared the magnetic susceptibilities of the samples having 5% and 57 % of the subspectrum with IS of 0.39 mm/s . In the heat-treated sample, the susceptibility increased by 10% that is too small change compared to what is expected for the increase of Peff from 4.9 $\mu_B$ to 5.9 $\mu_B$. With the weight loss taken into account this result would rather indicate the formation of an intermediate-spin state of $Fe^{3+}$ which is known for strongly distorted octahedral coordinations with two alternate ligands in *cis*-configuration[39].

## IV. CONCLUSION

Mössbauer spectroscopy was applied to study the mixed-valence ($Fe^{2+}$-$Co^{3+}$) PB analogues which displayed the mixed-orbital ground states of $Fe^{2+}$ ions. The ground state mixing originates from both the distortion isomerism and the varied composition of $Fe^{2+}$ nearest-neighbor environment. In the A-free PB analogues, water molecules enter the first coordination sphere of the $Fe^{2+}$ ions. There appears two kinds of anisotropic ligand configurations which are the intrinsic generant of the singlet and doublet orbital ground states. The $Fe^{2+}$ sites are thus classified into two types.

Distribution of the anionic vacancies (water-filled pores) over the framework is characterized by the order parameter for two long-range order models $Pm\bar{3}m$ or $Im\bar{3}m$. These models are relevant to the PB analogues of the 4:3 and 3:2 stoichiometries, respectively. Two water molecules within the first coordination sphere of $Fe^{2+}$ is the most populated configuration of the random model $Fm\bar{3}m$ and ordered models $Pm\bar{3}m$ or $Im\bar{3}m$. The short-range order event occurrence in PB analogues of the 3:2 and 4:3 stoichiometries favors the cis- and trans- conformations, respectively. Orbital singlet is the lowest in energy state for the cis-conformation. Accordingly, in the A-free ferrous cobalticyanide PB analogue, the Mössbauer spectra of $Fe^{2+}$ are dominated by the larger quadrupole-splitting component.

In the A-filled PB analogues, where the the water ligands are withdrawn from the $Fe^{2+}$ coordination sphere, the least anisotropic charge distribution attainable for the cases of A=Rb and Cs is the orbital doublet ground state. For A=Na and K, the thermally-induced interconversions between the doublet and singlet ground states were observed attributed to distortion isomerism. Charge-transfered states intrinsic in the PB analogues with negative thermal expansion[26] are suggested to be the source of the lattice distortions associated with the distortion isomerism. Asymmetry of Mössbauer spectra is attributed to the admixture of a small content (at the level of ∼5%) of the $Fe^{3+}$ species associated with the charge-transferred states.

Since the octahedral sites $FeN_6$ possess a higher symmetry than the sites $FeN_{6-n}(H_2O)_n$ we observe upon the insertion the A-ions into A free compounds that the value of Mössbauer QS drops in ferrous cobalticyanides similarly to the archetypal Prussian Blue $Fe_4[Fe(CN)_6]_3 \cdot 14H_2O$[20]. However, when the large-size A-ions (Cs, Rb) replace the small-size ones (Na,K) through ionic exchange we observe the larger QS associated with lower symmetry local distortion isomer; the sixth d-electron of the $Fe^{2+}$ cation is self-localized on a single sublevel (orbital singlet) of the $t_{2g}$ group owing to strong lattice distortions around the implanting sites of the low-mobility ions.

## V. ACKNOWLEDGEMENT

This work was partly supported by the Chinese Academy of Sciences Visiting Professorships for Senior International Scientists. Grant No. 2011T1G15. Financial support obtained from the Chinese Academy of Sciences for "100 Talents" Project, the National Natural Science Foundation of China (No. 11079036) and the Natural Science Foundation of Liaoning Province (No. 20092173) is also greatly acknowledged.

[1] K. Kato, Y. Moritomo, M. Takata, M. Sakata, M. Umekawa, N. Hamada, S. Ohkoshi, H. Tokoro, and K. Hashimoto, Phys. Rev. Lett. **91,** 255502 (2003).

[2] Ph. Gütlich, Y. Garcia, and H.A. Goodwin, Chem. Soc. Rev. **29**, 419-427 (2000).

[3] E. Coronado, M.C. Giménez-López, T. Korzeniak, G. Levchenko, F.M. Romero, A. Segura, V. García-Baonza, J.C. Cezar, F.M.F. de Groot, A. Milner. and M. Paz-Pasternak, J. Am. Chem. Soc. **130,** 15519-15532 (2008).

[4] C. Chong, M. Itoi, K. Boukheddaden, E. Codjovi, A. Rotaru, F. Varret, F.A. Frye, D.R. Talham, I. Maurin, D. Chernyshov, and M. Castro, Phys. Rev. **B 84,** 144102 (2011).

[5] A. B. Koudriavtsev, W. Linert, J. Struct. Chem. Engl. Transl. **51,** 335-365 (2010).

[6] Y. Moritomo, F. Nakada, H. Kamioka, T. Hozumi, and S. Ohkoshi, Phys. Rev. **B 75**, 214110 (2007).

[7] M. Kabir and K.J. VanVilet, Phys. Rev. **B 85**, 054431 (2012).

[8] A.I. Rykov, Y. Ueda, K. Nomura, and M. Seto, Phys. Rev. **B 79** 224114 (2009)**.**

[9] R. Latorre, C.R. Abeledo, R.B. Frankel, J.A. Costamagna, W.M. Reiff, E. Frank, J. Chem. Phys. **59** (1973) 2580-2585.

[10] U. Volland, J. Phys. Colloques, **41**, C1-309-C1310 (1980).

[11] G.R. Hoy, and F. de. S. Barros, Phys. Rev. **139**, A929-A934 (1965).

[12] P.G. Rasmussen and E.A. Meyers, Polyhedron **3** (1984) 183-190.

[13] E. Reguera, H. Yee-Madeira, S. Demeshko, G. Eckold, and J. Jimenez-Gallegos, Z. Phys. Chem., **223** (2009) 701-711.

[14] E. Reguera, H. Yee-Madeira, J. Fernández-Bertran, L. Nuñez, Transition Met. Chem., **24** (1999) 163-167.

[15] W. Kosaka, K. Nomura, K. Hashimoto, and S.-I. Ohkoshi, J. Am. Chem. Soc. **127**, 8590 (2005).

[16] J. F. Keggin, and F.D. Miles, Nature (London) **137** (1936) 577-578.

[17] A. Ludi, H.U. Güdel, Struct. Bonding, **14** (1973) 1-21.

[18] H.J. Buser, D. Schwarzenbach, W. Petter, and A. Ludi, Inorg. Chem. **16** (1977) 2704-2710.

[19] H. Tokoro, S.-I. Ohkoshi, T. Matsuda and K. Hashimoto, Inorg. Chem. **43** ( 2004) 5231-5236.

[20] A.I. Rykov, J. Wang, T. Zhang and K. Nomura, Hyperfine Interact. DOI 10.1007/s10751-012-0705-5 (in press).

[21] R.J. Evans, D.G. Rancourt, and M. Grodzicki, American Mineralogist **90** (2005) 187-198.

[22] U. Ganiel, Chem. Phys. Lett., 4 (1969) 87.

[23] R. Latorre, J.A. Costamagna, E. Frank, C.R. Abeledo, and R.B. Frankel, J. Inorg. Nucl. Chem. **41** (1979) 649-655.

[24] R. Ingalls, Phys. Rev. **133** (1964) A787-A795.

[25] P.B. Merrithew, P.G. Rasmussen, and D.H. Vincent, Inorg. Chem. **10** (1971) 1401-1406.

[26] T. Matsuda, J.E. Kim, K. Ohoyama, and Y. Moritomo, Phys.Rev. **B 79**, 172302 (2009).

[27] S. Adak, L.L. Daemen, M. Hartl, D. Williams, J. Summerhill, H. Nakotte, J. Solid St. Chem. **184**, 2854 (2011).

[28] M.W. Reiff, R.B. Frankel, B.F. Little, and G.J. Long, Chem. Phys. Lett. **28,** 68 (1974).

[29] A. Widmann, H. Kahlert, I. Petrovic-Prelevic, H. Wulff, J. V. Yakhmi, N. Bagkar, and F. Scholz, Inorg. Chem. **41** (2002) 5706-5715.

[30] S. Ayrault, B. Jimenez, E. Garnier, M. Fedoroff, D.J. Jones, and C. Loos-Neskovic, J. Solid St. Chem. **141** (1998) 475-485.

[31] C. Loos-Neskovic, S. Ayrault, V. Badillo, B. Jimenez, E. Garnier, M. Fedoroff, D.J. Jones, and B. Merinov, J. Solid St. Chem. **177** (2004) 1817-1828.

[32] F. Herren, P. Fischer, A. Ludi, and W. Hälg, Inorg. Chem. **19** (1980) 956-959.

[33] S.S. Kaye, J.R. Long, Catal. Today, **120** (2007) 311-316.

[34] V. Ksenofontov, A. B. Gaspar and P Gütlich, Topics in Current Chemistry, 2004, Volume 235, Spin Crossover in Transition Metal Compounds III, Pages 39-66.

[35] J.C. Wojdeł, I.P.R. Moreira, and F. Illas, J. Chem. Phys. **130,** 014702 (2009).

[36] D.S. Middlemiss, D. Portinari, C.P. Grey, C.A. Morrison, and C.C. Wilson, Phys. Rev. **B 81**, 184410 (2010).

[37] S. Hayami, Y. Shigeyoshi, M. Akita, K. Inoue, K. Kato, K. Osaka, M. Takata, R. Kawajiri, T. Mitani, and Y. Maeda, Angew. Chem. Int. Ed. **44**, 4899 (2005).

[38] P.T. Manoharan, B. Sambandam, R. Amasarani, B. Varghese, C.S. Gopinath, and K. Nomura, Inorg. Chem. Acta **374**, 586 (2011).

[39] P.J. van Koningsbruggen, Y. Maeda, H. Oshio, Top. Curr. Chem. **233**, 259 (2004).